Growth of amorphous selenium thin films: classical versus quantum mechanical molecular dynamics simulation

Growth of amorphous selenium thin films: classical versus quantum mechanical molecular dynamics simulation

J Hegedüs[1] and S Kugler[2,3]

[1] Department of Physics and Material Sciences Center, Philipps University Marburg, Renthof 5, D-35032 Marburg, Germany
[2] Department of Theoretical Physics, Budapest University of Technology and Economics, H-1521 Budapest, Hungary
[3] Department of Electronics and Computer Engineering, Tokyo Polytechnic University, Japan

Abstract

We present the first molecular dynamics simulation of the vacuum deposition of amorphous selenium films. We compare the classical, tight-binding and Hubbard-term corrected tight-binding molecular dynamics simulation methods. Densities, coordination defects, radial distribution functions, bond angles, dihedral angles, intrachain and interchain atomic correlations were investigated in the obtained amorphous films. Local atomic arrangements were compared to results of diffraction measurements.

1. Introduction

Recently, amorphous chalcogenide thin films have received particular attention due to their unique light-induced effects [1, 2]. Samples for experiments can either be grown by vacuum deposition techniques or prepared with rapid quenching. We focus on vacuum deposition where the starting compound is evaporated and condensed to a substrate. This process can be followed by an atomic-scale molecular dynamics (MD) simulation where the forces acting on the particles are calculated from a model interatomic interaction which can be either a classical empirical or a quantum mechanical description. The quality of the model interaction profoundly determines the results obtained by molecular dynamics simulation.

In this paper we compare three different types of interaction by growing amorphous selenium (a-Se) thin films. Amorphous selenium is considered as a model material for chalcogenide glasses. As far as we know no molecular dynamics investigation has been carried out on a-Se thin film growth yet. Our particular questions are the following. What are the differences in physical properties of the films simulated using various interatomic potentials? When should we use the more CPU time-consuming quantum mechanical description instead of the classical empirical one?
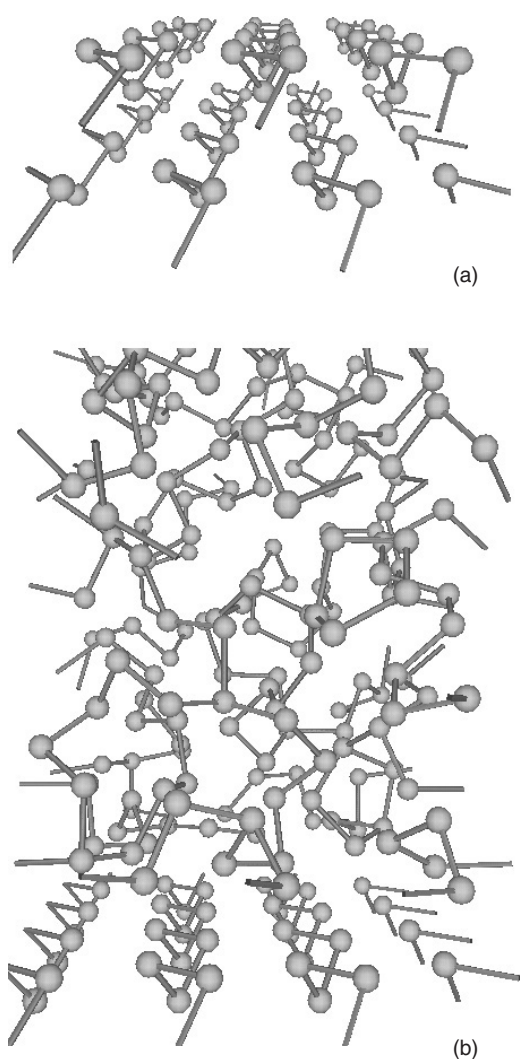
Figure 1. Snapshots of the substrate (a) and of an amorphous selenium film (b) after relaxation. The substrate consisted of six 12-member helical selenium chains. The three bottom chains were fixed to mimic the underlying bulk material. Dangling bonds at the border are displayed for a better visualizations of the periodic boundary conditions.

2. Simulation technique

Our simulation algorithm for atomic deposition has been already applied successfully for growing amorphous carbon [3], silicon [4] and selenium films [5]. An α-crystalline selenium lattice with chains directed perpendicular to the growth direction was chosen as the substrate model (figure 1(a)). It contained 72 selenium atoms of which 36 atoms were held fixed at the bottom part of the substrate. The dimensions of the substrate were 13.35 and 19.0 Å in the x and y directions where periodic boundary conditions were applied. The simulation cell was open along the z axis, i.e., in the growth direction. For integrating the Newton equations in the MD simulation we used the velocity Verlet algorithm [6]. The time step was chosen to be 1 fs.

The preparation conditions were identical in each case; only the interatomic interactions were different. The total kinetic energy of the atoms in the substrate was rescaled at every MD step in order to keep the substrate at a constant temperature ($T = 300$ K). We used the growing-substrate algorithm: as soon as atoms arrived at a substrate-atom closer than 3.5 Å they were treated also as a substrate-atom: their temperature was also controlled [7].

The incoming atoms were randomly positioned above the substrate and their initial velocity corresponded to an average kinetic energy of 1 eV with Maxwellian velocity distribution. Directions were determined by $\theta = 120° + p \times 60°$ and $\phi = p \times 360°$, where θ and ϕ are polar angles and p is a uniformly distributed random number between 0 and 1.

In the deposition process the frequency of the atomic injection was 125 fs^{-1}. The total bombardment period was 500 ps. The corresponding flux is orders of magnitude larger than the deposition rate commonly applied in experiments which usually corresponds to a couple of monolayers per second. We have compensated this deviation by the growing-substrate algorithm [7]. A 20 ps period followed the bombardment (no more incoming atoms) for structure relaxations.

3. Potentials

3.1. Classical empirical potential

For classical empirical simulations we have chosen the three-body potential developed by Oligschleger *et al* [8]. It employs two-body and three-body terms to describe correctly the two-fold coordinated nature of selenium structures. The potential was parameterized by fitting the binding energy of Se-clusters and crystalline phases to DFT calculations and experimental values. It was used to investigate the structure, relaxation and thermal properties of amorphous selenium [9–11].

3.2. Tight-binding model

Tight-binding models [12] for studying amorphous selenium have been widely used in recent years [13–16]. The tight-binding (TB) method preserves the quantum mechanical description of bonding when compared to empirical methods but its drawback is the higher computational cost. However, when comparing it with the *ab initio* techniques it is faster, but it has reduced transferability because of the approximations made. For our simulations we have chosen the model proposed by Molina *et al* [17] which has been tested in different phases and proved to give acceptable agreement with experiments. The total energy was computed by diagonalizing the hopping matrix [17].

3.3. Tight-binding model with Hubbard correction

In disordered phases of selenium the TB model developed by Molina *et al* [17] produces large charge transfer and favours coordination defect formations. To correct this discrepancy the authors introduced a Hubbard term [18], which increases the potential energy of the system if positive or negative charge accumulates on atoms. The Hubbard term can be taken into account either by perturbation theory [18] or by self-consistent field method. We have chosen the latter, which requires iterative solving where one can use the solution obtained in the previous MD step as the starting point for the actual MD step. Usually, only a few iterative steps were needed to obtain the solution in our simulation.

Table 1. Model, number of atoms in bulk (N_{bulk}), percentages of atoms with different coordination numbers (Z), and density ρ (g cm^{-3}). Experimental data were taken from [18, 19].

Model	N_{bulk}	$Z = 1$	$Z = 2$	$Z = 3$	ρ
CLASS	272	0.8%	88.3%	10.9%	4.21
TB-NOHUB	282	16.7%	46.6%	36.7%	4.31
TB-HUB	274	1.9%	92.0%	6.1%	4.27
Experiment			99.9%		4.47

4. Comparison of the structures

4.1. Densities, coordination defects

We denote the structural model prepared with the classical empirical potential by CLASS. Structures obtained using tight-binding models are named as TB-NOHUB (without Hubbard term) and TB-HUB (with Hubbard term). To eliminate surface and substrate effects [3], we took into account only a 33.0 Å thick layer with 5 Å above the substrate and at least 5 Å below the atom which had the largest z-coordinate. A typical snapshot after relaxation can be seen in figure 1(b). The number of atoms, densities and percentages of coordination defects inside the subsystem are shown in table 1. Densities are lower by 4%–5% than the experimental value [19], which can be attributed to the fact that preparational details affect the density: for example, our previous classical molecular-dynamics simulation study on a-Se thin film growth has shown that bombarding energy correlates with the final density of the amorphous films [5].

Two atoms are considered to be bonded if the distance between them is shorter than 2.8 Å. The most stable α-crystalline phase of selenium consists of helical chains parallel to each other, which means that every atom is two-fold coordinated. Other crystalline phases of selenium are built up from eight-member rings [20]. In the amorphous phase selenium chains can end or branch at coordination defects (one-fold or three-fold coordinated atoms). In liquid (close to the melting point) and glassy selenium their concentrations are very low [18, 21], i.e., chains of a thousand atoms can exist [19]. We have found that model TB-HUB gives the lowest defect concentration: it provides the most realistic modelling in this respect. Simulation of the amorphization by rapid quenching using the TB-HUB interaction can produce samples having more than 99% two-fold coordinated atoms [22]. By comparing the TB-NOHUB and TB-HUB models it turns out that the Hubbard term is essential for achieving low coordination defect density: in the TB-NOHUB model nearly every second atom introduces a coordination defect.

The dominant structural defect in model CLASS is the branching of selenium chains. Accordingly, this model has the lowest one-fold coordination defect density: it is below 1%. Coordination defects change the corresponding average bond length, too. Higher coordination number causes longer bond length (table 2). This correlation can be observed in all the models and its magnitude can even reach 10%.

4.2. Radial distribution functions

In figure 2, the radial distribution functions (RDFs) are depicted. Curves are obtained as time-averages during equilibrating the final structures at 300 K for 10 ps. The first peak describes the nearest-neighbour shell: model CLASS has the sharpest peak, whereas model TB-NOHUB has the broadest due to the overwhelming presence of coordination defects. In this model the peak position is also shifted to larger values compared to its counterparts because of the longer

Table 2. Influence of coordination number (Z) on average bond length (d_{bond}), bond angle (θ_{bond}), dihedral angle (γ) and number of interchain neighbours (N_{ICN}).

Model	Z	d_{bond} (Å)	θ (deg)	γ (deg)	N_{ICN}
	1	2.33			9.9
CLASS	2	2.36	102.5	80.0	8.0
	3	2.43	101.0	83.8	5.8
	1	2.38			9.0
TB-NOHUB	2	2.41	99.5	95.4	7.0
	3	2.45	99.0	93.6	5.4
	1	2.36			10.1
TB-HUB	2	2.42	101.5	85.6	7.8
	3	2.48	100.9	95.6	5.4

bond lengths associated with three-fold coordinated atoms. The second peaks correspond to second-neighbour distances. Model CLASS has a single peak at 3.6 Å; by contrast, in model TB-NOHUB two shoulders can be seen at 3.25 and 3.9 Å, which become more pronounced in model TB-HUB. For a better understanding of the curves we divided them into two components: corresponding either to interatomic distances between atoms in the same chain (intrachain–RDF) or in different chains (interchain–RDF). One can see that in model CLASS the interchain and intrachain peaks almost coincide at 3.6 and 3.7 Å. The first peak is much broader and has also a greater total area under the curve than the second peak. The shoulders seen in the total RDF in model TB-NOHUB and model TB-HUB are the consequences of the different peak positions of the interchain and intrachain curves. Furthermore, in model TB-NOHUB and model TB-HUB the interchain RDF has a small shoulder, i.e., a pre-peak at 3.25 Å. The intrachain curve is broadened in model TB-NOHUB due to the broad first-neighbour peak. We characterized the structures also by measuring the number of interchain neighbours, which is the number of atoms being closer than 4.5 Å to a given atom but being in a different chain (see figure 2, dotted line). We observed the decrease of the number of interchain neighbours with increasing coordination number (table 2). This is reasonable since the more neighbours an atom has the more intrachain second-nearest neighbours it has. That is why there will be less space left for interchain neighbours.

4.3. Bond angles

The bond angle distributions of the models differ significantly: the time-averaged distribution can be seen in figure 3. Bond angles were not larger than 115° in either model; however, we have observed very rarely thermally fluctuating bond angles which had could temporarily have values from 80° up to 180° in every model. Model TB-NOHUB has the smallest bond angle values. Due to the high number of three-fold coordination defects, model TB-NOHUB also has the largest area under the curve, which gives the average number of bond angles per atom. Model CLASS provides the sharpest peak: here the full width at half maximum (FWHM) is only 8°; in comparison, in model TB-NOHUB it is 18°. Model TB-HUB has a bimodal intrachain radial distribution function (figure 2) due to the corresponding bond angle distribution (figure 3). A similar bimodal structure has also been reported by Shimizu *et al* [14]. Furthermore, bond angles depend on the coordination number of the central atom: in every model two-fold coordinated atoms have larger average bond angles than three-fold coordinated atoms but this difference is very small: it is about 1–2% (see table 2).
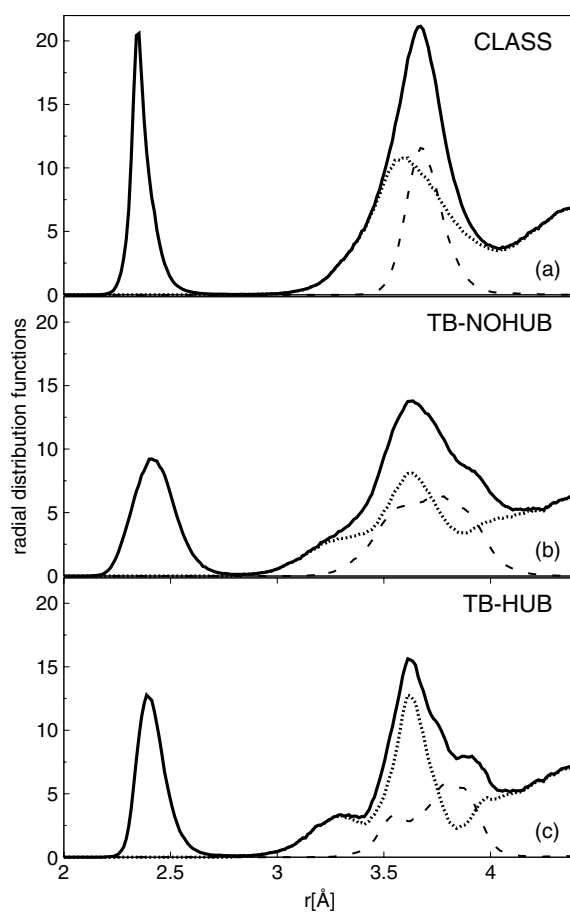
Figure 2. Radial distribution functions of our amorphous selenium models prepared by classical-empirical potential (a), tight-binding model without Hubbard term (b), and tight-binding model with Hubbard term (c). Solid lines represent the total radial distribution function, dotted and dashed lines correspond to the inter- and intrachain interatomic separations, respectively.

4.4. Correlation between bond angles and bond lengths

A correlation between bond angles and bond lengths of –Se–Se–Se– fragments can be observed in models CLASS and TB-NOHUB (figure 4). However, a monotonic dependence cannot be seen in model TB-HUB. To compare these results to experiments we have additionally analysed the structure of 512 molecules containing –Se–Se–Se– fragments. This systematic analysis of structural data has been carried out using the Cambridge Structural Database (CSD) [23], which is the world's largest database of experimentally determined crystal structures containing the results of x-ray and neutron diffraction studies. The CSD is designed as a critically evaluated numerical resource, containing three-dimensional atomic coordinates. The result of the search is shown in figure 5. Each point represents a measured bond angle as a function of bond length. The majority of the points fall in the expected region, i.e., around 2.35 Å and 102°. The minimum bond length is 2.09 Å, while the maximum is 2.58 Å. The bond angles lie inside the interval 79°–114°. Drawing a line of best fit (figure 4, thin solid line), a correlation can be observed, i.e., an increase of bond angle corresponds to a decrease of bond length (figure 4).
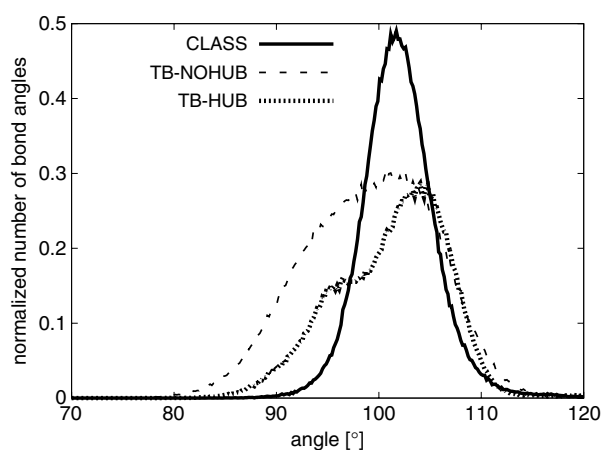
Figure 3. Bond angle distributions of our amorphous models. Model TB-HUB provides a bimodal distribution (dotted line) whereas model CLASS has the sharpest peak (solid line) while model TB-NOHUB the broadest (dashed line).
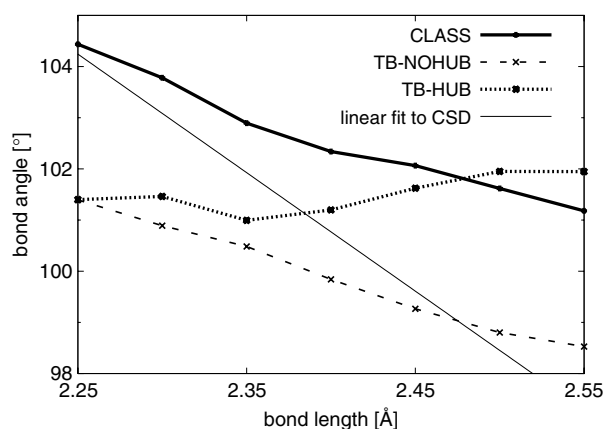

Figure 4. Bond angles of –Se–Se–Se– fragments correlate with their bond lengths in models CLASS (solid line) and TB-NOHUB (dashed line). However, model TB-HUB (dotted line) shows a non-monotonic bond angle dependence on the bond length values. The thin solid line represents the best linear fit (with $\sigma = 4.2°$) to the corresponding bond angle and bond length values obtained from the Cambridge Structural Database (see figure 5).

A similar result has been obtained for the case of silicon fragments [24]. This tendency can be also seen in models CLASS and TB-NOHUB, while a contrary behaviour is present in model TB-HUB. This suggest that although model TB-HUB performs as the best in all other aspects, it fails to describe correctly the dependence of bond lengths on bond angles.

4.5. Dihedral angles

In figure 6 a comparison of dihedral angle distributions of –Se–Se–Se–Se– fragments (obtained from the CSD, figure 6(a)) and of our models is shown (figure 6(b)). To improve the statistics we used 18° wide bins to create the dihedral angle distribution histogram of our models. Additionally, we modelled the random distribution of dihedral angles to measure
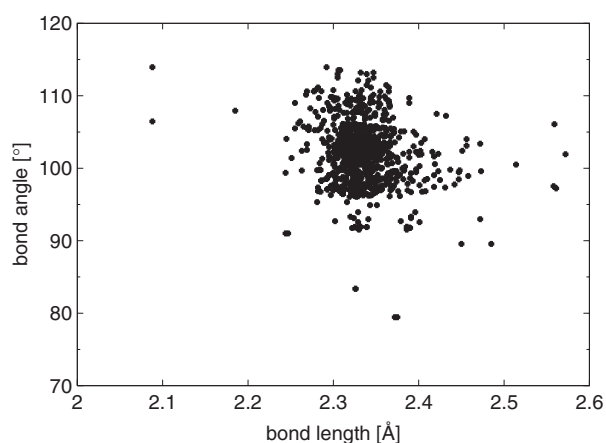
Figure 5. Bond angles versus bond lengths function of 512 –Se–Se–Se– fragments in different molecules. Note that fragments having bond lengths larger than 2.38 Å have mainly bond angles smaller than 105° while larger bond angles correspond to smaller bond lengths.
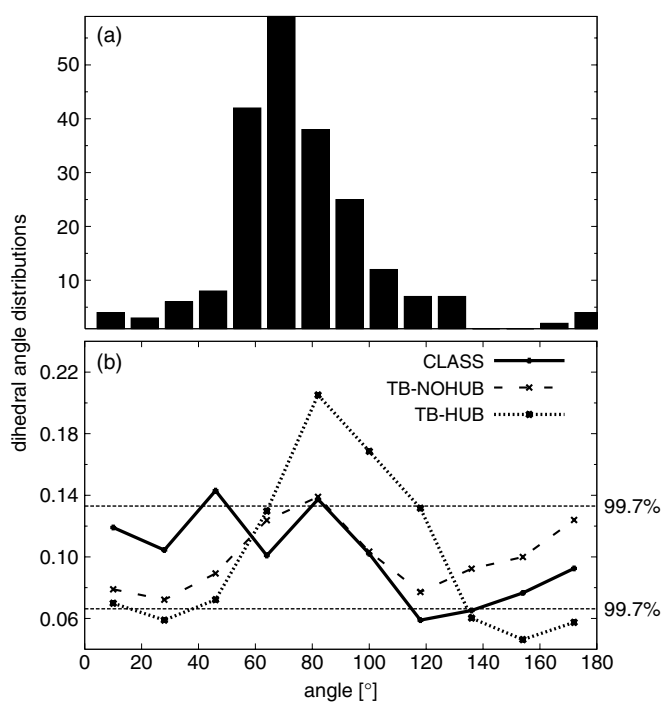

Figure 6. Dihedral angle distributions of –Se–Se–Se–Se– fragments in the CSD (a) and of our models (b). Line types are defined as in figure 3. Horizontal dashed lines represent the interval in which randomly distributed dihedral angles would lie with 99.7% probability. Only by points lying outside this interval can the corresponding dihedral angles be considered as significantly preferred or not preferred.

the significancy of the dihedral angle distributions obtained from the grown thin films. If the dihedral angles in our models were completely randomly distributed between 0° and 180° then the corresponding histogram values would lie between 0.133 and 0.066 (indicated by

dashed horizontal lines in figure 6(b)) with a probability higher than 99.7%. For modelling the completely randomly distributed dihedral angles, we assumed that the number of dihedral angles lying inside one bin has a binomial distribution. In this model calculation we assumed that the total number of dihedral angles is 300. We conclude that model CLASS does not prefer dihedral angles around 120° and prefers them around 40°. Model TB-HUB does not prefer them around 30° and 150°. All models significantly prefer dihedral angles around 80°. *Ab initio* calculations for amorphous [25] and liquid selenium near to melting point [26] have yielded dihedral angles similar to those in model TB-HUB. For comparison, the dihedral angles in α-selenium and α-monoclinic selenium crystalline phases are 100.7° and 103.1°, respectively [20]. Furthermore, the dihedral angle distribution of –Se–Se–Se–Se– fragments in the CSD is very similar to the dihedral angle distribution of model TB-HUB, but the peak position is shifted with ∼15° towards smaller values. Therefore, we consider model TB-HUB as the most realistic description in this respect.

We also analysed how coordination defects influence dihedral angles. Let us assume a chain segment of four selenium atoms: A–B–C–D. The corresponding average dihedral angle is influenced by the coordination number of atom B (see table 2). The most significant effect can be seen in model TB-HUB: the average dihedral angle increases by ∼10% with increasing coordination number.

5. Summary

We have grown amorphous selenium thin films using three different types of selenium interatomic interactions in our molecular dynamics simulations: one of them is based on a classical empirical three-body potential and the other two are of quantum mechanical origin. We analysed the structural properties of the obtained amorphous networks: significant differences were found in the radial distribution functions, bond angles, dihedral angles and coordination defects. Furthermore, we have presented statistics based on a large number of diffraction measurements on molecules containing selenium fragments. We observed an increase in bond length with decreasing bond angle. Only model TB-HUB did not reproduce this experimental result.

Overall, model TB-HUB seems to be the most realistic amorphous selenium network. Model TB-NOHUB is unacceptable due to it is high number of coordination defects.

Acknowledgments

References

[1] Tanaka Ke 1998 *Phys. Rev.* B **57** 5163
[2] Singh J and Shimakawa K 2003 *Advances in Amorphous Semiconductors* (London: Taylor and Francis)
[3] Kohary K and Kugler S 2001 *Phys. Rev.* B **63** 193404
[4] Kohary K and Kugler S 2004 *Mol. Simul.* **30** 17
[5] Hegedus J, Kohary K and Kugler S 2004 *J. Non-Cryst. Solids* **338** 283
[6] Allen M P and Tildesley D J 1990 *Computer Simulation of Liquids* Oxford

[7] Hegedus J 2003 *Master Thesis* Budapest University of Technology and Economics

[8] Oligschleger C, Jones R O, Reimann S M and Schober H R 1986 *Phys. Rev.* B **32** 1340

[9] Oligschleger C and Schon J C 1999 *Phys. Rev.* B **59** 4125

[10] Caprion D and Schober H R 2000 *Phys. Rev.* B **62** 3709

[11] Caprion D, Matsui J and Schober H R 2000 *Phys. Rev. Lett.* **85** 4293

[12] Goringe C M, Bowler D R and Hernandez E 1997 *Rep. Prog. Phys.* **60** 1447

[13] Bichara C, Pellegatti A and Gaspard J P 1994 *Phys. Rev.* B **49** 6581

[14] Shimizu F, Kaburaki H, Oda T and Hiwatari Y 1999 *J. Non-Cryst. Solids* **250** 433

[15] Koslowski T, Koblischke M and Blumen A 2002 *Phys. Rev.* B **66** 064205

[16] Raty J Y, Saul A, Gaspard J P and Bichara C 1999 *Phys. Rev.* B **60** 2441

[17] Molina D, Lomba E and Kahl G 1999 *Phys. Rev.* B **60** 6372

[18] Lomba E, Molina D and Alvarez M 2000 *Phys. Rev.* B **61** 9314

[19] Jovari P and Pusztai L 2001 *Phys. Rev.* B **64** 014205

[20] Donohue J 1974 *The Structures of The Elements* (New York: Wiley)

[21] Kresse G, Kirchhoff F and Gillan M J 1999 *Phys. Rev.* B **59** 3501

[22] Hegedus J, Kohary K and Kugler S 2005 *J. Optoelectron. Adv. Mater.* **7** 59

[23] Allen F H, Kennard O and Taylor R 1983 *Acc. Chem. Res.* **16** 146

[24] Kugler S and Varallyay Z 2001 *Phil. Mag. Lett.* **81** 569

[25] Hohl D and Jones R O 1991 *Phys. Rev.* B **43** 3856

[26] Kirchhoff F, Kresse G and Gillan M J 1998 *Phys. Rev.* B **57** 10482